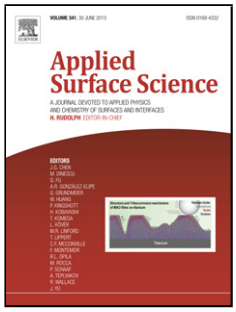

Title: Enhanced photoelectrochemical performance and photocatalytic activity of ZnO/TiO_2 nanostructures fabricated by an electrostatically modified electrospinning

Authors: Pierre G. Ramos, Edson Flores, Luis A. Sánchez, Roberto J. Candal, Mirabbos Hojamberdiev, Walter Estrada, Juan Rodriguez

PII: S0169-4332(17)32218-3
DOI: http://dx.doi.org/doi:10.1016/j.apsusc.2017.07.218
Reference: APSUSC 36752

To appear in: *APSUSC*

Received date: 28-2-2017
Revised date: 21-7-2017
Accepted date: 24-7-2017

Please cite this article as: Pierre G.Ramos, Edson Flores, Luis A.Sánchez, Roberto J.Candal, Mirabbos Hojamberdiev, Walter Estrada, Juan Rodriguez, Enhanced photoelectrochemical performance and photocatalytic activity of ZnO/TiO2 nanostructures fabricated by an electrostatically modified electrospinning, Applied Surface Sciencehttp://dx.doi.org/10.1016/j.apsusc.2017.07.218

Enhanced photoelectrochemical performance and photocatalytic activity of ZnO/TiO_2 nanostructures fabricated by an electrostatically modified electrospinning

Pierre G. Ramos[a], Edson Flores[a], Luis A. Sánchez[a], Roberto J. Candal[b], Mirabbos Hojamberdiev[d], Walter Estrada[a], and Juan Rodriguez[a,*]

[a]*Facultad de Ciencias, Universidad Nacional de Ingeniería, P.O. Box 31-139, Av. Túpac Amaru 210, Lima, Perú*

[b]*Instituto de Investigación e Ingeniería Ambiental, CONICET, Universidad Nacional de San Martín, Campus Miguelete, 25 de Mayo y Francia, 1650, San Martín, Provincia de Buenos Aires, Argentina*

[c]*Department of Natural and Mathematic Sciences, Turin Polytechnic University in Tashkent, Kichik Halqa Yo'li 17, Tashkent 100095, Uzbekistan*

*C*orresponding author:* jrodriguez@uni.edu.pe (J. Rodriguez)

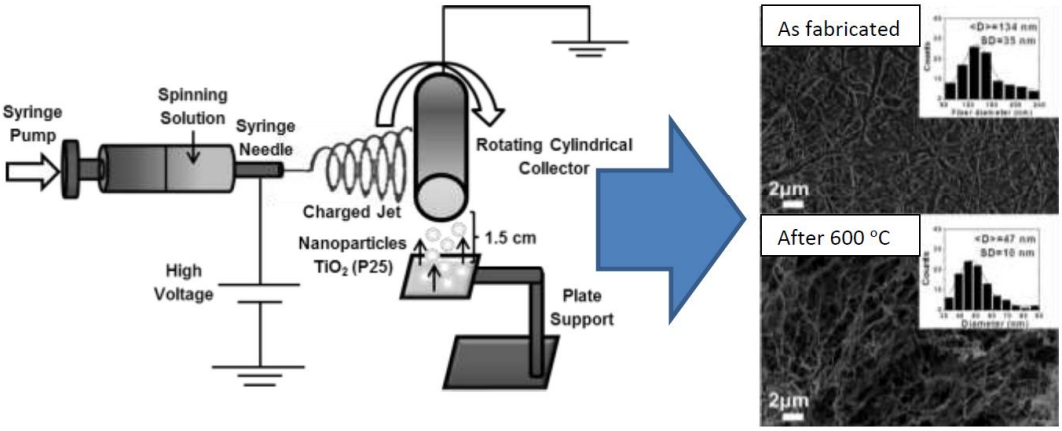

ABSTRACT:

In this work, ZnO/TiO_2 nanostructures were fabricated by an electrostatically modified electrospinning technique using zinc acetate and commercially available TiO_2-P25, polyvinyl alcohol, and a solvent. The ZnO/TiO_2 nanostructures were fabricated on fluorine-doped tin oxide (FTO) glass substrate by electrospinning of aqueous solution containing different amounts of zinc acetate. The TiO_2-P25 nanoparticles were immobilized within zinc acetate/PVA nanofibers. The precursor nanofibers obtained were converted into polycrystalline ZnO and ZnO/TiO_2 by calcination at 600°C. The structure and morphology of the obtained nanostructures were characterized by X-ray diffraction and field emission scanning electron microscopy, respectively. It was found that the TiO_2-P25 nanoparticles were attached to the ZnO nanostructures, and the mean diameter of the nanoparticles forming the nanostructures ranged from 31 to 52 nm with increasing the amount of zinc acetate. The incident photon-to-current efficiency (IPCE) spectra of the fabricated nanostructures were measured in a three-electrode cell. The photocatalytic activities of ZnO and ZnO/TiO_2 nanostructures were evaluated toward the decomposition of methyl orange.

The obtained results evidenced that the coupling of TiO_2 with ZnO enhanced the IPCE and improved the photocatalytic activity of ZnO. Particularly, the ZnO/TiO_2 nanostructures fabricated with a zinc acetate-to-PVA ratio of 2:3 exhibited the highest IPCE and photocatalytic activity.

KEYWORDS: Zinc oxide; Titanium dioxide, Electrospinning; Nanostructures; Photocatalytic activity

Introduction

Water pollution with organic dyes, detergents and pesticides has been an impetus for fundamental as well as applied research in the area of environmental remediation [1,2]. Photocatalysis phenomenon favors a green technique with great potential for the complete elimination of hazardous chemical pollutants in contaminated water and air owing to its efficiency, broad applicability, and environmentally friendliness [3]. So far, various metal oxides such as TiO_2, ZnO, CuO, MgO, WO_3, etc. have been demonstrated to be the promising photocatalytic materials [4,5], highlighting particularly ZnO and TiO_2 due to their size-tunable physicochemical properties, high photocatalytic activities, and lower cost [6,7]. Currently, the key focus on improving the efficiency of photocatalysts is to inhibit the recombination of photogenerated charge carriers (electron and holes). Thus, many researchers have explored various approaches to improve efficiency, including doping with transition metals or non-metals [8-11], coupling with other semiconductors to form composites [12-14], and morphological modification [15,16]. According to the studies dealing with the combination of different semiconductors, the coupling of ZnO with TiO_2 improved the photocatalytic activity for the degradation of organic pollutant due to effective charge separation [17]. Furthermore, the photocatalytic activity of the photocatalyst can also be improved by enlarging its specific surface area [18]. Thus, nanofibers can be suitable because of their high surface area-to-volume ratio, extremely long length, and small diameter. Several techniques such as template synthesis, phase separation, self-assembly, and electrospinning have been applied to fabricate the nanofibers [19]. Among them, electrospinning has been widely used to produce the nanofibers from polymeric precursor solution by applying an electrical potential between the end of an injection needle and a collector where the nanofibers are deposited [20,21]. Jin *et al.* [22] found that the electrospun nanofibers can double the specific surface area of the traditional thin films. A number of reports have previously demonstrated the formation of the ZnO/TiO_2 nanofibers by applying electrospinning technique using precursors of ZnO and TiO_2 [23,24]. However, the fabrication of the ZnO/TiO_2 nanofibers using TiO_2-P25 nanopowders attached to ZnO was not reported yet. The aim of this work is

to enhance the photocatalytic activity of ZnO nanofibers by coupling with commercial TiO_2-P25 nanopowders [25] through *in situ* adherence during the electrospinning process. Moreover, we demonstrate the influence of TiO_2 nanoparticles and zinc acetate content (zinc acetate-to-PVA mass ratio) on the morphology, crystallinity, photoelectrochemical performance, and photocatalytic activity for methyl orange degradation of ZnO/TiO_2 nanostructures deposited on fluorine-doped tin oxide (FTO) glass substrate by an electrostatically modified electrospinning technique. The crystallinity, morphologies, and microstructures of the fabricated nanostructures were analyzed by X-ray diffraction (XRD) and field emission scanning electron microscopy (FE-SEM), respectively. The incident photon-to-current efficiency (IPCE) of the fabricated nanostructures was evaluated in a three-electrode cell using a platinum wire and Ag/AgCl as a counter electrode and a reference electrode, respectively.

Materials and methods

Materials

Polyvinyl alcohol (M_W = 61,000 g·mol^{-1}, Sigma-Aldrich), zinc acetate dehydrate ($Zn(CH_3COO)_2{\cdot}2H_2O$, Merck), and commercially available TiO_2-P25 nanopowders (Degussa) were used as starting materials.

Fabrication

The precursor nanofibers were fabricated by the following procedure: an aqueous solution of PVA (14 wt%) was first prepared by dissolving 7.0 g of PVA powder in 43g of warm deionized water. Then different amounts of zinc acetate (ZnAc) were slowly added to 10g of the PVA solution in order to obtain diverse spinning solutions with different ZnAc-to-PVA mass ratios (3:2, 1:1, 2:3 and 1:2). The spinning solution was homogenized by stirring at 60°C for 3 h. The electrospinning parameters were optimized after running a series of experiments. The obtained spinning solution was immediately transferred into a plastic syringe equipped with a blunt-ended 23-gauge stainless steel needle, which was connected to a high-voltage power supply. The electrical potential applied was 62 kV. The fabrication and deposition of the precursor nanofibers were conducted by a homemade electrospinning apparatus under ambient

conditions using fluorine-doped tin oxide (FTO) glass as a rotating collector substrate that was placed 10 cm away from the tip of the needle. The feeding rate of the electrospinning solution (2 $ml \cdot h^{-1}$) was controlled with a syringe pump, and the deposition time was 2 h. The adhesion of TiO_2-P25 nanoparticles within the PVA-zinc acetate nanofibers was achieved *in situ* during the electrospinning process by electrostatic induction, as shown in Fig. 1. During 2 h of electrospinning, 25 mg of TiO_2-P25 nanoparticles was distributed every 30 min on a metal plate at a distance of 1.5 cm from the collector substrate. In order to remove the polymer after the electrospinning process and to obtain ZnO and ZnO/TiO_2 nanostructures, the deposited precursor nanofibers were initially dried at 120°C for 6 h and then calcined at 600°C for 3 h.

Characterization

The obtained nanostructures were characterized by X-ray diffraction (XRD) using a Philips X'PERT MPD with Cu Kα radiation (λ = 1.5418 Å) in the 2θ scan range from 20 to 80°. The morphologies and microstructures of the as-spun precursor nanofibers as well as ZnO and ZnO/TiO_2 nanostructures were observed by using a Supra 40VP field emission scanning electron microscope (ZEISS) equipped with an energy dispersive X-ray spectrometer (EDX). The incident photon-to-current efficiency (IPCE) spectra of the ZnO and ZnO/TiO_2 nanostructures were measured by using a PG580 potentiostat/galvanostat (Uniscan Instruments) in a three-electrode cell using the fabricated nanostructures as a working electrode, a platinum wire as a counter electrode, Ag/AgCl electrode immersed in 0.1M KCl solution as a reference electrode, 0.1N NaOH as an electrolytic solution, and a 400-1000W Xe lamp coupled with an Oriel Cornerstone 130 monochromator (Oriel Instruments) as a light source. The light intensity was in the range of 0.10 - 2.10 $mW \cdot cm^{-2}$. The photocatalytic activities of the fabricated nanostructures were evaluated by the degradation of methyl orange (MO) under UV light irradiation. The applied light source was a 220W OSRAM Ultravitalux lamp with a measured radiation intensity of 70 $W \cdot m^{-2}$ in the UV-A range. Prior to irradiation, 3.0 mg of the fabricated nanostructures was dispersed in 50 mL aqueous solution of methyl orange with an initial concentration of 3 ppm under magnetic stirring for 30 min to

ensure an adsorption-desorption equilibrium. During the irradiation, 3 mL of the suspension was taken out every 1 h for the subsequent analysis of methyl orange concentration by a Lambda 25 UV–vis spectrophotometer (PerkinElmer) at 462 nm. The photocatalytic activities of the ZnO and ZnO/TiO_2 nanostructures fabricated with different ZnAc-to-PVA ratios in the spinning solutions were compared.

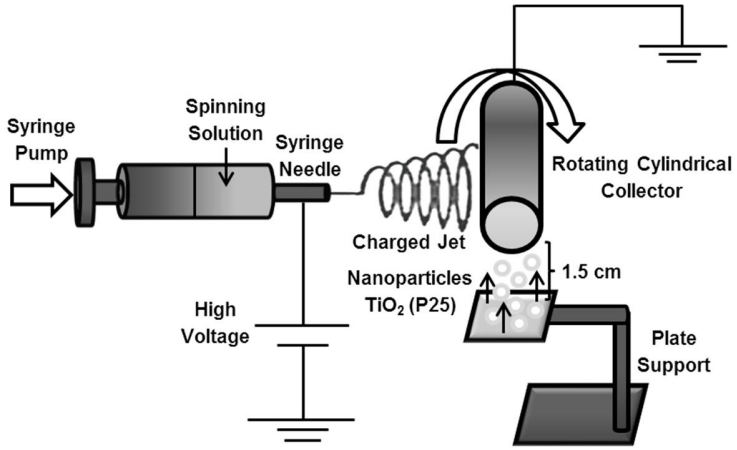

Fig. 1. Schematic diagram of an electrostatically modified electrospinning process applied to produce the precursor nanofibers of ZnO/TiO_2 nanostructures.

Results and discussion

Fig. 2 shows the FE-SEM images of the as-spun precursor fibers of ZnO fabricated using the spinning solution with a zinc acetate-to-PVA ratio of 2:3 before and after calcination at 600°C. As shown, the diameters of the precursor fibers fabricated using the spinning solutions with a ZnAc-to-PVA ratio of 2:3 were approximately 134 nm (Fig. 2a). After calcination, the diameters of the ZnO nanostructures became smaller compared to that of the precursor fibers due to the decomposition of PVA and the crystallization of ZnO during calcination [26, 27]. Fig. 3 shows the FE-SEM images of the precursor fibers of the TiO_2/ZnAc/PVA, indicating that the relatively smooth and rounded fibers were obtained. The FE-SEM image shows that, as indicated by white dashed circles, the TiO_2-P25 nanoparticles were attached to all fibers fabricated by electrospinning using the spinning solutions with different ZnAc-to-PVA ratios. The precursor fibers of ZnO/TiO_2 nanostructures fabricated with ZnAc-to-PVA ratios of 1:2 and 2:3 (Figs. 3a and b) do not clearly show the presence of the TiO_2 nanoparticles. Possibly, the TiO_2 nanoparticles

may be located among the fibers or completely coated by the polymer. In Figs. 3c and d, the precursor fibers of the ZnO/TiO_2 nanostructures fabricated with ZnAc-to-PVA ratios of 1:1 and 3:2 show that the TiO_2 nanoparticles were not only coated by the polymer but also adhered at the fibers in the form of agglomerates. This phenomenon may be associated with the increment of electrostatic attraction between the particles and the fibers as the conductivity of the fibers precursor solution increases. The conductivity of the solution increased with the concentration of ZnAc [28], leading to higher attraction between the TiO_2 particles and the spinning solutions with ZnAc-to-PVA ratios of 1:1 and 3:2. Thus, it will attract a higher amount of TiO_2 nanoparticles. Moreover, with increasing the amount of zinc acetate in the spinning solution, the diameters of the precursor fibers enlarged from 85 to 228 nm. It should be noted that as the amount of zinc acetate increases the diameter of the precursor fibers also increases and the distribution becomes broader. This is the result of the increment in the viscosity of the spinning solution as zinc acetate increases due to the gelation of zinc acetate (658 cP for 1:2 < 690 cP for 2:3 < 722 cP for 1:1 < 752 cP for 3:2). The increment in the viscosity can lead to non-uniform ejection of the jet [27,29], which in turn produces a broad distribution of the diameters of the precursor fibers.

On the other hand, comparing the precursor fibers of ZnO with the precursor fibers of the TiO_2/ZnAc/PVA fabricated with a ZnAc-to-PVA ratio of 2:3, a decrease in the fiber diameters was noted. This can be due to the presence of the collector/plate system (shown in Fig. 1). According to previous reports [30,31], the introduction of new objects and the use of different collectors directly influence the size and morphology of the fabricated fibers. Therefore, this new system collector/plate generates a slight distortion in the field electric lines thereby causing further stretching of the polymer jet which reduced the fiber diameters [32].

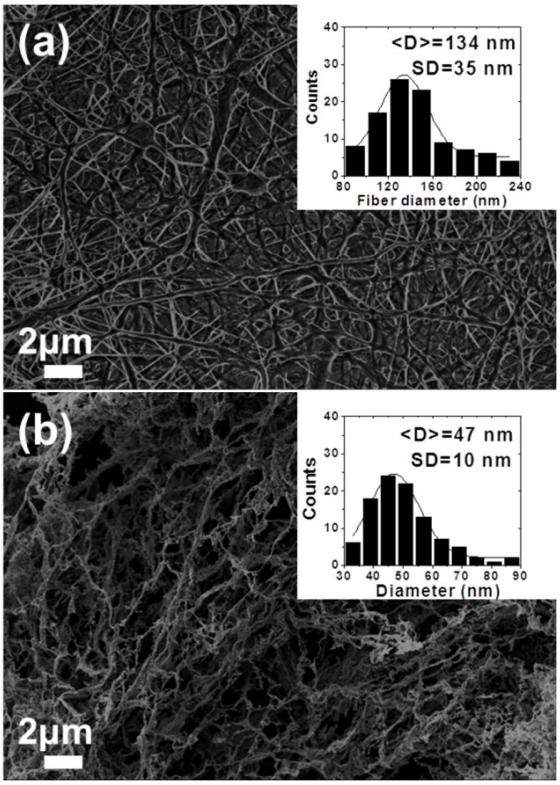

Fig. 2. FE-SEM images of the precursor fibers fabricated using the spinning solution with a ZnAc-to-PVA ratio of 2:3 before (a) and after (b) calcination at 600°C. The diameter distributions with corresponding standard deviations (SD) of the fabricated precursor fibers (a) and the mean diameter of the final ZnO skeleton nanostructures (b) are shown as insets.

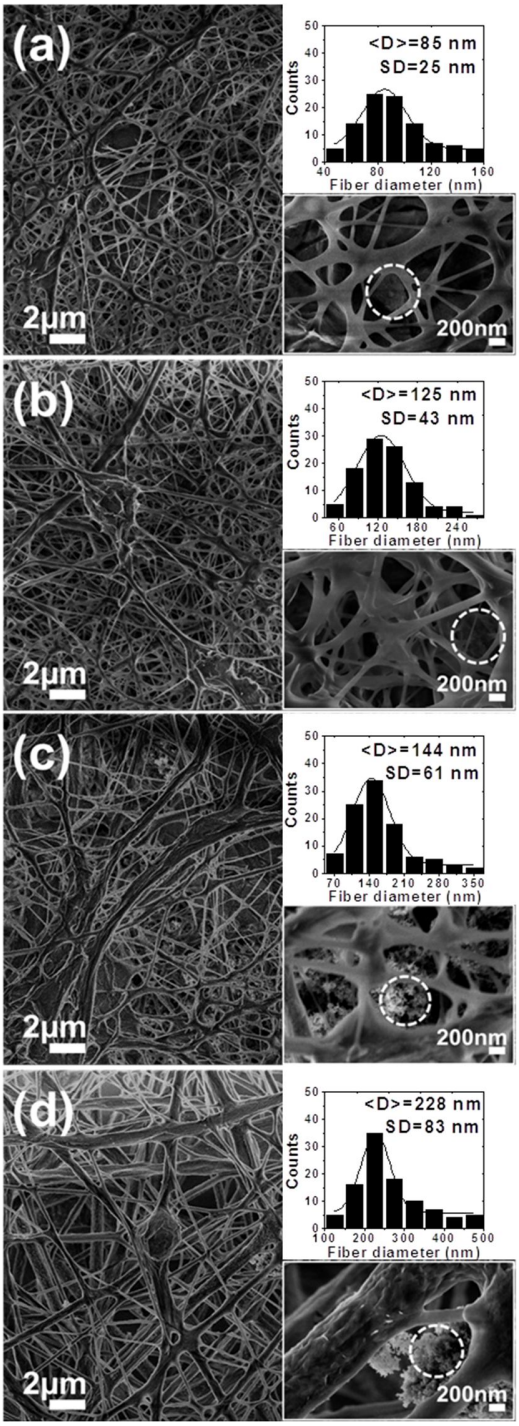

Fig. 3. FE-SEM images of the precursor fibers of TiO_2/ZnAc/PVA fabricated using the spinning solutions with different ZnAc-to-PVA ratios: (a) 1:2, (b) 2:3, (c) 1:1, and (d) 3:2. The diameter distributions with corresponding standard deviations (SD) of the fabricated precursor fibers are shown as insets.

The FE-SEM images of the ZnO/TiO_2 nanostructures obtained by calcination of the fabricated precursor fibers at 600°C are shown in Fig. 4. It is clear that although the PVA was completely decomposed, the formation of the ZnO/TiO_2 nanostructures was mainly governed by the amount of zinc acetate in the spinning solution. The mean diameter of the nanoparticles forming the ZnO/TiO_2 nanostructures increases with increasing the amount of zinc acetate in the following order: 31 nm for 1:2 < 36 nm for 2:3 < 45 nm for 1:1 < 52 nm for 3:2. The obtained results suggest that the dispersed zinc acetate clusters in the PVA matrix of the precursor fibers can act as nucleation sites upon calcination [33], resulting in the growth of ZnO nanocrystals on the fibers. According to Muangban and Jaroenapibal [34], the ZnO nanostructures can also be obtained with a lower concentration (1:2) because the ZnO nuclei are well separated from each other, thus unable to form primary particles during the calcination process, leading to the formation of nanofibers with a large area of ordered atomic arrangement (Fig. 4a). In contrast, the higher precursor concentrations lead to the formation of nanofibers with larger nanoparticles connected along the fiber axis. This is due to the formation of primary particles during the calcination process prior to the complete decomposition of the polymer matrix (Fig. 4d). Further, the mean diameter of the nanoparticles from the ZnO/TiO_2 nanostructures is smaller than that of the nanoparticles from the ZnO nanostructures despite the fact that both of them were fabricated using the same spinning solution with a zinc acetate-to-PVA ratio of 2:3. This is related to the decrease in the fiber diameter due to the use of the plate, where the TiO_2 nanoparticles were placed for *in situ* adhesion on the precursor fibers of ZnO during the electrospinning process. The EDS spectra of the ZnO/TiO_2 nanostructures shown in Fig. 4 confirm the complete decomposition of the PVA, the crystallization of ZnO after calcination of the precursor fibers, and the adhesion of the TiO_2 nanoparticles. The peaks associated with zinc, titanium, and oxygen can be seen in the EDS spectra. The atomic and weight percentages of titanium in the selectively analyzed area increased with increasing the amount of zinc acetate in the following order for atomic percentage: 0.44% for 1:2 < 0.86% for 2:3 < 1.78% for 1:1 < 1.94% for 3:2 and for weight percentage: 0.55% for 1:2 < 1.10% for 2:3 < 2.09% for 1:1 < 2.85% for

3:2. These results suggest that a higher amount of the precursor salt (zinc acetate) in the spinning solution increases its conductivity [35,36] and therefore attracts a higher amount of the TiO_2 nanoparticles that were *in situ* deposited on the precursor fibers of zinc acetate/PVA during the electrospinning process.

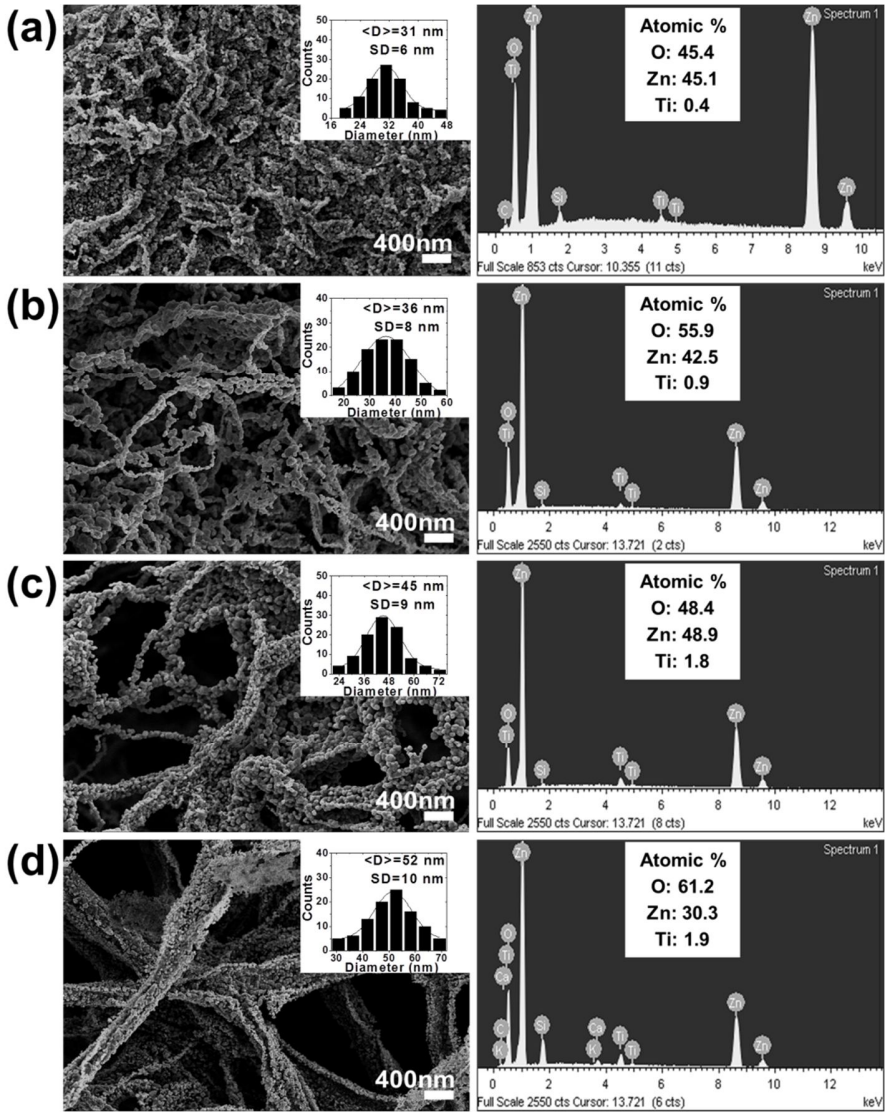

Fig. 4. FE-SEM images (*left sides*) and EDS spectra (*right side*) of the ZnO/TiO_2 nanostructures obtained by calcination of the precursor fibers prepared using the spinning solutions with different ZnAc-to-PVA ratios: (a) 1:2, (b) 2:3, (c) 1:1, and (d) 3:2. The nanoparticle distributions with corresponding standard deviations (SD) are shown as insets.

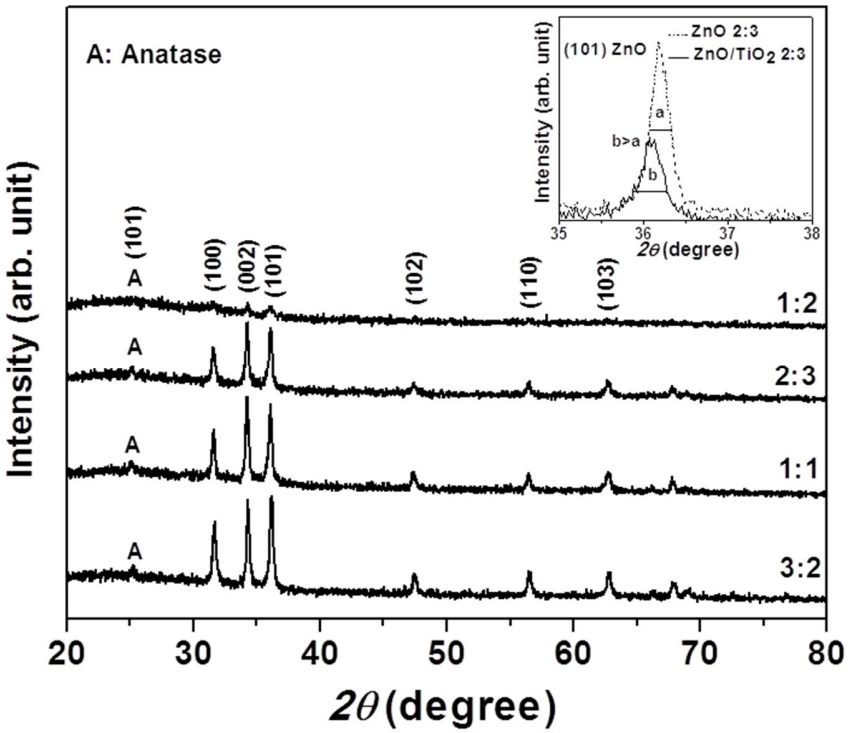

Fig. 5. XRD patterns of the ZnO/TiO_2 nanostructures fabricated using the spinning solutions with various ZnAc-to-PVA ratios (1:2, 2:3, 1:1 and 3:2). The (101) diffraction peak of ZnO is comparatively shown in the inset.

The XRD patterns of the ZnO/TiO_2 nanostructures fabricated by calcination of the precursor fibers at 600°C are shown in Fig. 5. The XRD patterns of the fabricated nanostructures contain six main diffraction peaks corresponding to the (100), (002), (101), (102), (110), and (103) crystallographic planes of hexagonal wurtzite structure of ZnO (ICDD PDF# 36-1451) and one main diffraction peak corresponding to the (101) crystallographic plane of anatase TiO_2 (ICDD PDF# 21-1276). Other diffraction peaks of anatase TiO_2-P25 were not observed possibly because of its small amount leading to a low intensity in the diffraction patterns. Similar intensity of the diffraction peaks indicates no preferential growth direction in the particles of ZnO present in the ZnO/TiO_2 nanostructures. Moreover, comparing the diffraction peaks of the ZnO/TiO_2 nanostructures with those of the ZnO nanostructures (for example the (101) diffraction peak showed in the inset of Figure 5), there was an increment in the Full Width at Half Maximum (FWHM) and reduction in the intensity in the case with TiO2. This result

is due the decrease in particle size (Figure 4) compared to those obtained for the ZnO nanostructures, indicating that the presence of TiO_2 nanoparticles hindered the growing of ZnO cristalites. This phenomenon is a clear indication of the strong interaction between TiO_2 nanoparticles and ZnO precursor fibers.

The incident photon-to-current conversion efficiency (IPCE) spectra of the ZnO and ZnO/TiO_2 nanostructures are plotted in Figs. 6a and b as a function of wavelength. As shown, the ZnO and ZnO/TiO_2 nanostructures fabricated using the spinning solution with a zinc acetate-to-PVA mass ratio of 2:3 exhibited the highest IPCE value in the wavelength range from 330 to 420 nm compared with other nanostructures fabricated using the spinning solution with zinc acetate-to-PVA mass ratios of 1:2, 1:1 and 3:2. Although the ZnO and ZnO/TiO_2 nanostructures fabricated with a zinc acetate-to-PVA mass ratio of 3:2 contained the highest amount of zinc acetate, they showed the lowest IPCE values in the wavelength range from 330 to 420 nm. Depending on zinc acetate-to-PVA mass ratio, the IPCE values of the ZnO and ZnO/TiO_2 nanostructures increased in the following order: 4% for 3:2 < 7% for 1:2 < 28% for 1:1 < 31% for 2:3 for ZnO and 7% for 3:2 < 9% for 1:2 < 31% for 1:1 < 43% for 2:3 for ZnO/TiO_2 at about 350 nm. The results also show an increase in the IPCE values of the ZnO/TiO_2 nanostructures compared with the IPCE values obtained for the ZnO nanostructures. This can be due to the *in situ* adhesion of TiO_2-P25 nanoparticles within the ZnO nanostructures during the electrospinning process. According to previous studies [37,38], this can assist to improve the efficiency of light absorption, electron injection, and efficiency of collection, thus enhancing the IPCE value. Furthermore, the main difference in the IPCE values of all the fabricated nanostructures is presumably attributed to the enhanced light absorption, electron transfer rate, and delayed charge recombination [39,40], which depend on the morphology, adhesion of TiO_2-P25 nanoparticles to the substrates, and specific surface area of the fabricated nanostructures [41]. In the case of the ZnO and ZnO/TiO_2 nanostructures fabricated with zinc acetate-to-PVA mass ratios of 3:2, 1:1 and 2:3, the number of nanofibers was increased as the amount of

zinc acetate in the spinning solution was decreased, covering the surface of FTO glass (Fig. 4). It is thought that the reasons for the highest efficiency of the nanostructures fabricated with a zinc acetate-to-PVA mass ratio of 2:3 are good adhesion of TiO_2-P25 nanoparticles, the presence of a number of nanofibers, small crystal size resulting in a large specific surface area, and enhanced light absorption [40,42]. In contrast, the nanostructures fabricated with a zinc acetate-to-PVA mass ratio of 3:2 showed the lowest efficiency due to large crystal size and the presence of a few nanofibers (Fig. 4d).

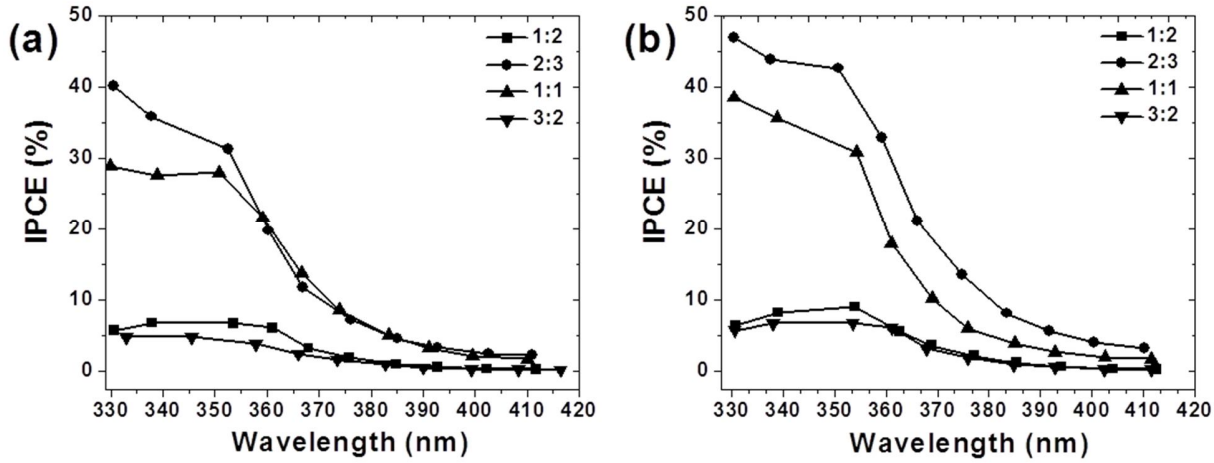

Fig. 6. IPCE curves of (a) ZnO and (b) ZnO/TiO_2 nanostructures fabricated using the spinning solutions with different ZnAc-to-PVA ratios (1:2, 2:3, 1:1 and 3:2).

In order to elucidate the effect of coupling of TiO_2-P25 nanoparticles with ZnO nanostructures, the photocatalytic activities of the ZnO and ZnO/TiO_2 nanostructures were evaluated by the photodegradation of methyl orange in aqueous solution under UV-A irradiation, and the results are plotted in Fig. 7. Blank experiment (i.e., only light irradiation without catalysts) showed that MO was hardly degraded under the control experimental conditions, corroborating the degradation reaction was truly driven by a photocatalytic process. Figs. 7a and b show the change in the methyl orange concentration in aqueous solution containing the ZnO and ZnO/TiO_2 nanostructures fabricated by calcination of the precursor fibers obtained using the spinning solutions with different zinc acetate-to-PVA ratios. The results indicate that the ZnO nanostructures fabricated with a zinc acetate-to-PVA mass

ratio of 2:3 show the highest photocatalytic activity compared with other ZnO nanostructures fabricated with zinc acetate-to-PVA mass ratios of 1:2, 1:1 and 3:2. It is known that the photocatalytic activity of one-dimensional nanostructures generally depends on crystallinity [43] and specific surface area that in turn relies on particle size [44]. It is suggested that the reason why the ZnO nanostructures fabricated with a zinc acetate-to-PVA mass ratio of 2:3 have the highest photocatalytic activity because its particle size (~ 47 nm) is smaller than that of the ZnO nanostructures fabricated with zinc acetate-to-PVA mass ratios of 3:2 and 1:1; therefore, the sample has a larger specific surface area. As shown, methyl orange molecules were not completely decomposed during 6 h of photocatalytic reaction. This extended time was applied because of a less amount of photocatalyst used (approximately 0.06 g/L). As reported by Singh et al. [45], the photodegradation time was increased with decreasing the load of the ZnO nanostructures. Fig. 7a shows that depending on zinc acetate-to-PVA mass ratio, the methyl orange degradation rate constant of the ZnO nanostructures increases in the following order: 0.095 h^{-1} for 3:2 < 0.181 h^{-1} for 1:2 < 0.257 h^{-1} for 1:1 < 0.284 h^{-1} for 2:3. It can be inferred that the photocatalytic activity of the ZnO nanostructures is greatly improved by the TiO_2-P25 nanoparticles *in situ* adhered to the ZnO nanostructures during the electrospinning process. The highest photocatalytic activity was obtained for the ZnO/TiO_2 nanostructures fabricated with a zinc acetate-to-PVA mass ratio of 2:3, and the methyl orange degradation rate constant of the ZnO/TiO_2 nanostructures increases in the following order: 0.106 h^{-1} for 3:2 < 0.198 h^{-1} for 1:2 < 0.430 h^{-1} for 1:1 < 0.762 h^{-1} for 2:3. The results of the photocatalytic activity test of the ZnO and ZnO/TiO_2 nanostructures are in good agreement with their IPCE data (Fig. 6).

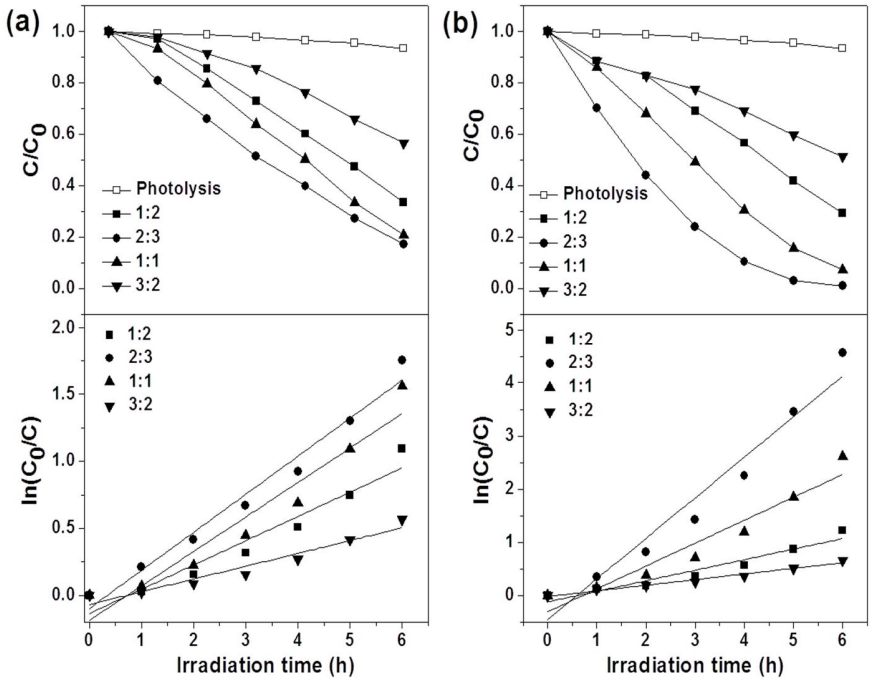

Fig. 7. Change in the MO concentration and rate constants of the photodegradation of MO over (a) ZnO and (b) ZnO/TiO_2 nanostructures fabricated using the spinning solutions with different ZnAc-to-PVA ratio (1:2, 2:3, 1:1 and 3:2).

The improvement of photocatalytic activity of the ZnO/TiO_2 nanostructures is related to the role of TiO_2-P25 nanoparticles adhered to the ZnO nanostructures. Fig. 8 shows the mechanisms of charge separation and photocatalytic reaction for the ZnO/TiO_2 nanostructures. As illustrated in the scheme, when the nanostructure is irradiated with UV light with a photon energy greater than or equal to the band gap of ZnO and TiO_2, the electrons (e^-) in the valence band (VB) are excited to the conduction band (CB) with generation simultaneous of the same number of holes (h^+) in the VB (Eq. (1)). The electron transfer occurs from the CB of light-activated ZnO to the CB of light-activated TiO_2, and conversely, the hole transfer takes place from the VB of TiO_2 to that of ZnO (Eq. (2)) [39,46]. The photogenerated electrons and holes in the ZnO/TiO_2 photocatalysts could inject into reaction medium and participate in chemical reactions, in which electrons reduced the dissolved molecular oxygen to produce $O_2^{\bullet -}$ ($O_2 + e \rightarrow O_2^{\bullet -}$), while holes oxidized H_2O molecular to yield $\bullet OH$ ($h^+ + H_2O \rightarrow \bullet OH + H^+$). Because of the separation

of the photogenerated electrons and holes, more $O_2^{\bullet -}$ radicals and holes were produced, improving the photocatalytic activity. The hydroxyl radical $(\bullet OH)$ is an extremely strong oxidation for the partial or complete mineralization of organic chemicals. This efficient charge separation increases the lifetime of the photogenerated charge carriers and reduces the recombination of the hole–electron pairs in the composite nanostructures. Therefore, increases the photocatalytic activity of ZnO/TiO_2 nanostructures obtained in this research.

$$ZnO/TiO_2 \xrightarrow{h\nu} ZnO(e_{CB}^- \dots h_{VB}^+)/TiO_2(e_{CB}^- \dots h_{VB}^+) \quad \text{(a)}$$

$$ZnO(e_{CB}^- \dots h_{VB}^+)/TiO_2(e_{CB}^- \dots h_{VB}^+) \quad \text{(b)}$$

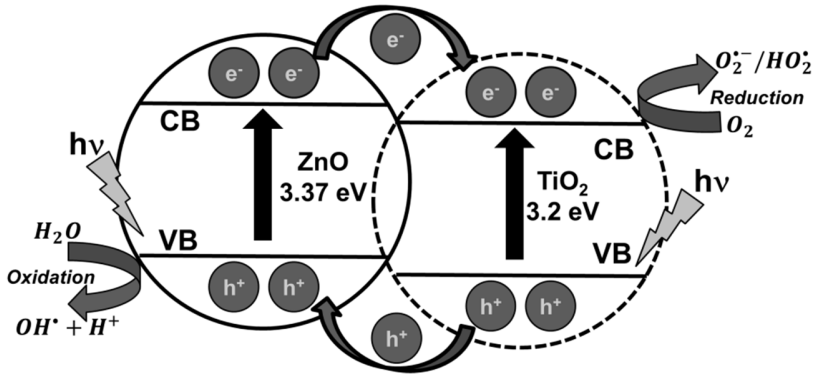

Fig. 8. A schematic diagram illustrating the principle of charge separation and photocatalytic activity of the ZnO/TiO_2 composite nanostructures system.

4. Conclusions

The ZnO/TiO_2 nanostructures were fabricated by an electrostatically modified electrospinning technique and their photoelectrochemical performance and photocatalytic activities for the photodegradation of methyl orange in aqueous solution were studied. The zinc acetate-to-PVA mass ratio and adhered TiO_2-P25 nanoparticles were found to play an important role on morphology tailoring, photoelectrochemical performance, and photocatalytic activity of the ZnO/TiO_2 nanostructures. The

mean diameter of the nanoparticles of the ZnO/TiO_2 nanostructures ranged from 31 to 52 nm and was increased as the amount of zinc acetate was further increased. The ZnO/TiO_2 nanostructures fabricated using the spinning solution with a zinc acetate-to-PVA ratio of 2:3 exhibited the highest IPCE value and the highest photocatalytic activity for the photodegradation of methyl orange in aqueous solution. The enhancement in the photoelectrochemical performance and photocatalytic activity of the ZnO/TiO_2 nanostructures is attributed to the high efficiency in both light utilization and separation of photogenerated charge carriers. The electrostatically modified electrospinning technique demonstrated here can be extended further for fabricating other semiconductor-based composite nanostructures that can be effectively applied for environmental remediation and energy conversion.

Acknowledgements

This work was supported by the FINCyT Project (no. 140-FINCYT-IB-2013). PGR would like to thank the Peruvian Council for Science and Technology (CONCYTEC) for the Scholarship. The authors are grateful to Dr. Claudia Marchi for her excellent technical assistance in scanning electron microscopy observation. MH would also like to thank the World Academy of Sciences (TWAS) for Visiting Expert Programme (F.R. 32402182000). RJC is member of CONICET; financial support from PICT 2014 2386 is appreciated.

References

[1] D. Ravelli, D. Dondi, M. Fagnoni, A. Albini, Photocatalysis. A multi-faceted concept for green chemistry, Chem. Soc. Rev. 38 (2009) 1999–2011.

[2] S. Teixeira, P.M. Martins, S. Lanceros-Méndez, K. Kühn, G. Cuniberti, Reusability of photocatalytic TiO2 and ZnO nanoparticles immobilized in poly(vinylidene difluoride)-co trifluoroethylene, Appl. Surf. Sci. 384 (2016) 497–504.

[3] H.R. Pant, C.H. Park, B. Pant, L.D. Tijing, H.Y. Kim, C.S. Kim, Synthesis, characterization, and photocatalytic properties of ZnO nano-flower containing TiO_2 NPs, Ceram. Int. 38 (2012) 2943–2950.

[4] T. Senthil, S. Anandhan, Structure–property relationship of sol–gel electrospun ZnO nanofibers developed for ammonia gas sensing, J. Colloid Interface Sci. 432 (2014) 285–296.

[5] C. Feng, C. Wang, P. Cheng, X. Li, B. Wang, Y. Guan, J. Ma, H. Zhang, Y. Sun, P. Sun, J. Zheng, G. Lu, Facile synthesis and gas sensing properties of La_2O_3–WO_3 nanofibers, Sens. Actuators B 221 (2015) 434–442.

[6] S.A. Mozaffari, M. Ranjbar, E. Kouhestanian, H.S. Amoli, M.H. Armanmehr, An investigation on the effect of electrodeposited nanostructured ZnO on the electron transfer process efficiency of TiO_2 based DSSC, Mater. Sci. Semicond. Process. 40 (2015) 285–292.

[7] M.Y. Guo, M.K. Fung, F. Fang, X.Y. Chen, A.M.C Ng, A.B. Djurišić, W.K. Chan, ZnO and TiO_2 1D nanostructures for photocatalytic applications, J. Alloys Compd. 509 (2011) 1328–1332.

[8] W. Zeng, X. Yang, M. Shang, X. Xu, W. Yang, H. Hou, Fabrication of Mg-doped ZnO nanofibers with high purities and tailored band gaps, Ceram. Int. 42 (2016) 10021–10029.

[9] J.C. Conesa, Band structures and nitrogen doping effects in zinc titanate photocatalysts, Catal. Today 208 (2013) 11–18.

[10] S. An, B.N. Joshi, M.W. Lee, N.Y. Kim, S.S. Yoon, Electrospun graphene-ZnO nanofiber mats for photocatalysis applications, Appl. Surf. Sci. 294 (2014) 24–28.

[11] M. Zhu, C. Zhai, L. Qiu, C. Lu, A.S. Paton, Y. Du, M.C. Goh, New Method to Synthesize S-Doped TiO_2 with Stable and Highly Efficient Photocatalytic Performance under Indoor Sunlight Irradiation, ACS Sustain. Chem. Eng. 3 (2015) 3123–3129.

[12] A. Hamrouni, N. Moussa, A. Di Paola, L. Palmisano, A. Houas, F. Parrino, Photocatalytic activity of binary and ternary SnO_2–ZnO–$ZnWO_4$ nanocomposites, J. Photochem. Photobiol. 309 (2015) 47–54.

[13] P.P. Dorneanu, A. Airinei, N. Olaru, M. Homocianu, V. Nica, F. Doroftei, Preparation and characterization of NiO, ZnO and NiO–ZnO composite nanofibers by electrospinning method, Mater. Chem. Phys. 148 (2014) 1029–1035.

[14] C. Li, X. Zhang, W. Dong, Y. Liu, High photocatalytic activity material based on high□porosity ZnO/CeO_2 nanofibers, Mater. Lett. 80 (2012) 145–147.

[15] S. Wei, S. Wang, Y. Zhang, M. Zhou, Different morphologies of ZnO and their ethanol sensing property, Sens. Actuators B 192 (2014) 480–487.

[16] Y. Yamin, N. Keller, V. Keller, WO_3-modified TiO_2 nanotubes for photocatalytic elimination of methylethylketone under UVA and solar light irradiation, J. Photochem. Photobiol. A 245 (2012) 43–57.

[17] G. Panthi, M. Park, H.-Y Kim, S.-Y. Lee, S.-J. Park, Electrospun ZnO hybrid nanofibers for photodegradation of wastewater containing organic dyes: a review, J. Ind. Eng. Chem. 21 (2015) 26–35.

[18] H.U. Lee, S.Y. Park, S.C. Lee, J.H. Seo, B. Son, H. Kim, H.J. Yun, G.W. Lee, S.M. Lee, B. Nam, J.W. Lee, Y.S. Huh, C. Jeon, H.J. Kim, J. Lee, Highly photocatalytic performance of flexible 3 dimensional (3D) ZnO nanocomposite, Appl. Catal. B 144 (2014) 83–89.

[19] S. Ramakrishna, K. Fujihara, W.-E. Teo, T.-C. Lim, Z. Ma, An introduction to electrospinning and nanofibers, World Scientific Publishing, Singapore, 2005.

[20] B. Ghorani, N. Tucker, Fundamentals of electrospinning as a novel delivery vehicle for bioactive compounds in food nanotechnology, Food Hydrocolloid 51 (2015) 227–240.

[21] D. Alipour, A.R. Keshtkar, M.A. Moosavian, Adsorption of thorium(IV) from simulated radioactive solutions using a novel electrospun $PVA/TiO_2/ZnO$ nanofiber adsorbent functionalized with mercapto groups: Study in single and multi-component systems, Appl. Surf. Sci. 366 (2016) 19–29.

[22] L. Jin, T. Wang, M.-L. Zhu, M.K. Leach, Y.I. Naim, J.M. Corey, Z.-Q. Feng, Q. Jiang, Electrospun fibers and tissue engineering, J. Biomed. Nanotechnol. 8 (2012) 1–9.

[23] C.C. Pei, W.W.-F. Leung, Photocatalytic degradation of Rhodamine B by TiO_2/ZnO nanofibers under visible-light irradiation, Sep. Purif. Technol. 114 (2013) 108–116.

[24] C.C. Pei, W.W.-F. Leung, Enhanced photocatalytic activity of electrospun TiO_2/ZnO nanofibers with optimal anatase/rutile ratio, Catal. Commun. 37 (2013) 100–104.

[25] J. Cabrera, H. Alarcón, A. López, R. Candal, D. Acosta, J. Rodriguez, Synthesis, characterization and photocatalytic activity of 1D TiO_2 nanostructures, Water. Sci. Technol. 70 (2014) 972–979.

[26] K. Thangavel, A. Balamurugan, T. Venkatachalam, E.R. Kumar, Structural, morphological and optical properties of ZnO nanofibers, Superlattices Microstruct. 90 (2016) 45–52.

[27] P.G. Ramos, N.J. Morales, R.J. Candal, M. Hojamberdiev, J. Rodriguez, Influence of zinc acetate content on the photoelectrochemical performance of zinc oxide nanostructures fabricated by electrospinning technique, Nanomater. Nanotechno. 6 (2016) 1847980416663679.

[28] A. Rogina, Electrospinning process: Versatile preparation method for biodegradable and natural polymers and biocomposite systems applied in tissue engineering and drug delivery, Appl. Surf. Sci. 296 (2014) 221–230.

[29] A. Khalil, R. Hashaikeh, Electrospinning of nickel oxide nanofibers: process parameters and morphology control, Mater. Charact. 95 (2014) 65–71.

[30] J. Walser, S.J. Ferguson, Oriented nanofibrous membranes for tissue engineering applications: Electrospinning with secondary field control, J. Mech. Behav. Biomed. Mater. 58 (2016) 188–198.

[31] J.H. Lee, D.W. Shin, K.B. Nam, Y.H. Gim, H.S. Ko, D.K. Seo, G.H. Lee, Y.H. Kim, S.W. Kim, T.S. Oh, J.B. Yoo, Continuous bundles of aligned electrospun PAN nano-fiber using electrostatic spiral collector and converging coil, Polym. 84 (2016) 52–58.

[32] P.G. Ramos, N.J. Morales, S. Goyanes, R.J. Candal, J. Rodríguez, Moisture-sensitive properties of multi-walled carbon nanotubes/polyvinyl alcohol nanofibers prepared by electrospinning electrostatically modified method, Mater. Lett. 185 (2016) 278–281.

[33] N. Sangkhaprom, P. Supaphol, V. Pavarajarn, Fibrous zinc oxide prepared by combined electrospinning and solvothermal techniques, Ceram. Int. 36 (2010) 357–363.

[34] J. Muangban, P. Jaroenapibal, Effects of precursor concentration on crystalline morphologies and particle sizes of electrospun WO_3 nanofibers, Ceram. Int. 40 (2014) 6759–6764.

[35] F.E. Ahmed, B.S. Lalia, R. Hashaikeh, A review on electrospinning for membrane fabrication: challenges and applications, Desalin. 356 (2015) 15–30.

[36] R. Sarbatly, D. Krishnaiah, Z. Kamin, A review of polymer nanofibres by electrospinning and their application in oil–water separation for cleaning up marine oil spills, Mar. Pollut. Bull. 106 (2016) 8–16.

[37] R. Murugan, V.J. Babu, M.M. Khin, A.S. Nair, S. Ramakrishna, Synthesis and photocatalytic applications of flower shaped electrospun ZnO–TiO_2 mesostructures, Mater. Lett. 97 (2013) 47–51.

[38] H.R. Pant, C.H. Park, B. Pant, L.D. Tijing, H.Y. Kim, C.S. Kim, Synthesis, characterization, and photocatalytic properties of ZnO nano-flower containing TiO_2 NPs, Ceram. Int. 38 (2012) 2943–2950.

[39] D. Ramírez-Ortega, A.M. Meléndez, P. Acevedo-Peña, I. González, R. Arroyo, Semiconducting properties of ZnO/TiO_2 composites by electrochemical measurements and their relationship with photocatalytic activity, Electrochim. Acta 140 (2014) 541–549.

[40] J. Fang, H. Fan, H. Tian, G. Dong, Morphology control of ZnO nanostructures for high efficient dye-sensitized solar cells, Mater. Charac. 108 (2015) 51–57.

[41] V. Thavasi, V. Renugopalakrishnan, R. Jose, S. Ramakrishna, Controlled electron injection and transport at materials interfaces in dye sensitized solar cells, Mater. Sci. Eng. R-Rep. 63 (2009) 81–99.

[42] S. Hu, B. Wang, M. Zhu, Y. Ma, Z. Lv, H. Wang, High-performance 1D type-II TiO_2@ZnO core-shell nanorods arrays photoanodes for photoelectrochemical solar fuel production, Appl. Surf. Sci. 403 (2017) 126–132.

[43] X. Dong, P. Yang, Y. Liu, C. Jia, D. Wang, J. Wang, L. Chen, Q. Che, Morphology evolution of one-dimensional ZnO nanostructures towards enhanced photocatalysis performance, Ceram. Int. 42 (2016) 518–526.

[44] A.C. Dodd, A.J. McKinley, M. Saunders, T. Tsuzuki, Effect of particle size on the photocatalytic activity of nanoparticulate zinc oxide, J. Nanopart. Res. 8 (2006) 43–51.

[45] P. Singh, K. Mondal, A. Sharma, Reusable electrospun mesoporous ZnO nanofiber mats for photocatalytic degradation of polycyclic aromatic hydrocarbon dyes in wastewater, J. Colloid Interface Sci. 394 (2013) 208–215.

[46] X. Zheng, D. Li, X. Li, J. Chen, C. Cao, J. Fang, J. Wang, Y. He, Y. Zheng, Construction of ZnO/TiO_2 photonic crystal heterostructures for enhanced photocatalytic properties, Appl. Catal. B 168 (2015) 408–415.

Figure captions

Fig. 1. Schematic diagram of an electrostatically modified electrospinning process applied to produce the precursor nanofibers of ZnO/TiO_2 nanostructures.

Fig. 2. FE-SEM images of the precursor fibers fabricated using the spinning solution with a ZnAc-to-PVA ratio of 2:3 before (a) and after (b) calcination at 600°C. The diameter distributions with corresponding standard deviations (SD) of the fabricated precursor fibers (a) and the nanoparticles forming the ZnO nanostructures (b) are shown as insets.

Fig. 3. FE-SEM images of the precursor fibers of TiO_2/ZnAc/PVA fabricated using the spinning solutions with different ZnAc-to-PVA ratios: (a) 1:2, (b) 2:3, (c) 1:1, and (d) 3:2. The diameter distributions with corresponding standard deviations (SD) of the fabricated precursor fibers are shown as insets.

Fig. 4. FE-SEM images (left sides) and EDS spectra (right side) of the ZnO/TiO_2 nanostructures obtained by calcination of the precursor fibers prepared using the spinning solutions with different ZnAc-to-PVA ratios: (a) 1:2, (b) 2:3, (c) 1:1, and (d) 3:2. The nanoparticle distributions with corresponding standard deviations (SD) are shown as insets.

Fig. 5. XRD patterns of the ZnO/TiO_2 nanostructures fabricated using the spinning solutions with various ZnAc-to-PVA ratios (1:2, 2:3, 1:1 and 3:2). The (101) diffraction peak of ZnO is comparatively shown in the inset.

Fig. 6. IPCE curves of (a) ZnO and (b) ZnO/TiO_2 nanostructures fabricated using the spinning solutions with different ZnAc-to-PVA ratios (1:2, 2:3, 1:1 and 3:2).

Fig. 7. Change in the MO concentration and rate constants of the photodegradation of MO over (a) ZnO and (b) ZnO/TiO_2 nanostructures fabricated using the spinning solutions with different ZnAc-to-PVA ratio (1:2, 2:3, 1:1 and 3:2).

Fig. 8. A schematic diagram illustrating the principle of charge separation and photocatalytic activity of the ZnO/TiO_2 composite nanostructures system.